CHEMISTRY OF MATERIALS

pubs.acs.org/cm

Article

Synthesis and Aqueous Solution Properties of Shape-Shifting Stimulus-Responsive Diblock Copolymer Nano-Objects

Oliver J. Deane, James Jennings, Thomas J. Neal, Osama M. Musa, Alan Fernyhough, and Steven P. Armes*

Cite This: https://doi.org/10.1021/acs.chemmater.1c02096

Read Online

ACCESS | Metrics & More | Article Recommendations | Supporting Information

ABSTRACT: We report the synthesis of poly(*N*-(2-acryloyloxyethyl)pyrrolidone)-poly(4-hydroxybutyl acrylate) ($PNAEP_{85}$-$PHBA_x$) diblock copolymer nano-objects via reversible addition−fragmentation chain transfer (RAFT) aqueous dispersion polymerization of 4-hydroxybutyl acrylate (HBA) at 30 °C using an efficient two-step one-pot protocol. Given the relatively low glass transition temperature of the PHBA block, these nano-objects required covalent stabilization prior to transmission electron microscopy (TEM) studies. This was achieved by core crosslinking using glutaraldehyde. TEM analysis of the glutaraldehyde-fixed nano-objects combined with small-angle X-ray scattering (SAXS) studies of linear nano-objects confirmed that pure spheres, worms or vesicles could be obtained at 20 °C in an acidic aqueous solution by simply varying the mean degree of polymerization (x) of the PHBA block. Aqueous electrophoresis, dynamic light scattering and TEM studies indicated that raising the dispersion pH above the pK_a of the terminal carboxylic acid group located on each PNAEP chain induced a vesicle-to-sphere transition. ^{1}H NMR studies of linear $PNAEP_{85}$-$PHBA_x$ nano-objects indicated a concomitant increase in the degree of partial hydration of PHBA chains on switching from pH 2-3 to pH 7-8, which is interpreted in terms of a surface plasticization mechanism. Rheological and SAXS studies confirmed that the critical temperature corresponding to the maximum worm gel viscosity could be tuned from 2 to 50 °C by adjusting the PHBA DP. Such tunability is expected to be useful for potential biomedical applications of these worm gels.

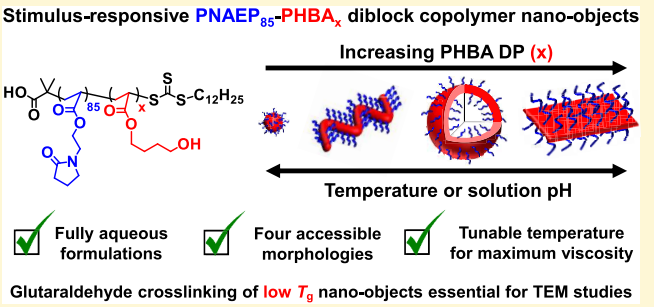

INTRODUCTION

It is well known that AB diblock copolymers can self-assemble in solution to form a range of sterically stabilized nanoparticles.[1−4] Depending on the relative volume fractions of the two blocks,[1] the copolymer morphology can be spheres,[1] worms[4,5] or vesicles.[6] However, traditional postpolymerization processing routes to such nano-objects usually require co-solvents and are invariably conducted in dilute solution.[1,5,7,8] These are important constraints that have severely limited potential commercial applications. In contrast, polymerization-induced self-assembly (PISA) enables the efficient synthesis of block copolymer nano-objects of controllable size, morphology, and surface composition directly in the form of concentrated dispersions in a wide range of polar[4,9−11] or non-polar[12,13] solvents. PISA involves chain extension of a soluble homopolymer precursor using a suitable second monomer in an appropriate solvent, with the latter being chosen so that the growing second block becomes insoluble at some critical chain length, thus leading to the formation of diblock copolymer nano-objects.[14−19] In principle, such nanoparticles offer a wide range of potential applications, including new biocompatible hydrogels for cell culture and long-term storage,[10,20,21] microencapsulation of proteins and enzymes within vesicles,[22−27] bespoke Pickering emulsifiers,[28] novel flocculants,[29] dispersants for agrochemical actives such as azoxystrobin,[30] and new lubricants for the formulation of ultralow-viscosity automotive engine oils.[31] The majority of the PISA literature involves reversible addition−fragmentation chain transfer (RAFT) polymerization.[32−40] This chemistry is based on the principle of rapid reversible chain transfer: an organosulfur-based CTA is used to produce well-defined block copolymers with low dispersities and predictable mean DPs.[41−43]

Recently, we reported the RAFT aqueous solution polymerization of *N*-(2-acryloyloxyethyl) pyrrolidone (NAEP) to produce various homopolymers and block copolymers.[44] Subsequently, a trithiocarbonate-capped poly(*N*-(2-acryloyloxyethyl)pyrrolidone) precursor was employed for the RAFT aqueous emulsion polymerization of styrene, *n*-

Received: June 17, 2021

butyl acrylate (*n*BA), and mixtures thereof.[45] The mean particle diameter and glass-transition temperature could be varied over a wide range by adjusting the target DP and comonomer composition of the structure-directing block. However, only kinetically trapped spheres could be obtained and the highly hydrophobic nature of their core-forming chains ensured that such nanoparticles did not exhibit any thermoresponsive behavior.

According to the PISA literature, RAFT aqueous dispersion polymerization often leads to thermoresponsive block copolymer nano-objects.[46−54] This is not particularly surprising because water-miscible monomers lead to more weakly hydrophobic structure-directing blocks than water-immiscible monomers.[10,55] In this context, we recently reported two examples of thermoresponsive diblock copolymers of fixed composition that can form spheres, worms or vesicles in an aqueous solution simply by adjusting the solution temperature.[18,56] In both cases, spheres are formed at subambient temperature, worms are produced at around ambient temperature, and vesicles are observed on heating above ambient temperature. Variable temperature ^{1}H NMR spectroscopy studies indicate that this remarkable behavior is the result of subtle changes in the degree of hydration of the weakly hydrophobic structure-directing block,[18,56] which was chosen to be poly(2-hydroxypropyl methacrylate) (PHPMA) in the first study and a statistical copolymer comprising 80 mol % 4-hydroxybutyl acrylate (HBA) and 20 mol % diacetone acrylamide (DAAM) in the second study. In the latter case, significantly greater chain mobility exhibited by the HBA-rich block led to thermoreversible sphere/worm and worm/vesicle transitions, whereas the corresponding transitions observed for PHPMA-based nano-objects exhibited strong hysteresis. Unfortunately, the HBA-rich block has a relatively low T_g, which prevented transmission electron microscopy (TEM) studies of the copolymer morphologies. In principle, this technical issue can be addressed using cryo-TEM.[57−59] However, the weakly hydrophobic nature of HBA-rich chains leads to a relatively high degree of hydration, which minimizes electron contrast with the frozen aqueous phase and leads to poor-quality images. Byard and co-workers addressed this problem by reacting the pendent methyl ketone groups on DAAM repeat units with a water-soluble crosslinker (adipic acid dihydrazide).[18] Such covalent stabilization enables TEM studies, but introducing the DAAM comonomer reduces the thermoresponsive behavior exhibited by the HBA-rich structure-directing block. In principle, the maximum thermoresponsive character should be obtained by omitting the DAAM comonomer from the PISA formulation to produce purely PHBA-based nano-objects. However, this approach requires the identification of a suitable alternative crosslinking protocol to enable the assignment of copolymer morphologies by conventional TEM. This is one of the main objectives of the present study.

Herein, we report the two-step one-pot synthesis of a series of new thermoresponsive pyrrolidone-functional diblock copolymer nano-objects via RAFT aqueous dispersion homopolymerization of HBA using PNAEP as a nonionic hydrophilic steric stabilizer (see Scheme 1).[44,45] For this highly efficient new PISA formulation, we explore the following four questions. Can a single diblock copolymer composition be identified that can form spheres, worms, or vesicles simply by varying the solution temperature? If so, can the local maximum in dispersion viscosity corresponding to the presence of linear worms be tuned over a wide range of temperature by systematic variation of the diblock copolymer composition? Given that each steric stabilizer chain contains a terminal carboxylic acid, do these nano-objects exhibit pH-responsive behavior via end-group ionization? Finally, can a robust new crosslinking strategy be developed to enable conventional TEM studies of such nano-objects?

Scheme 1. Two-Step One-Pot Synthesis of PNAEP$_{85}$-PHBA$_x$ Diblock Copolymer Nano-Objects via RAFT Aqueous Dispersion Polymerization of HBA at 30 °C Using a [PNAEP$_{85}$]/[KPS] Molar Ratio of 5.0 and a [KPS]/[AsAc] Molar Ratio of 1.0 [N.B. "KPS" Denotes $K_2S_2O_8$ and "AsAc" Denotes Ascorbic Acid]

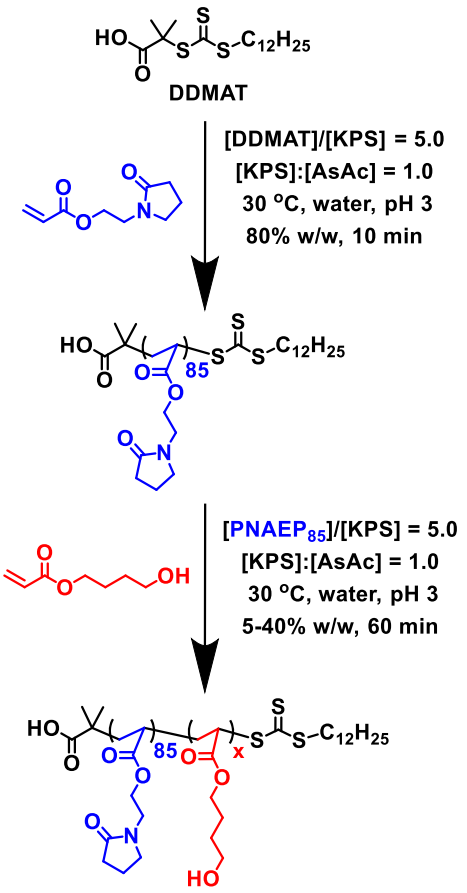

RESULTS AND DISCUSSION

A series of PNAEP precursors were prepared via RAFT aqueous solution polymerization of NAEP using DDMAT as a RAFT agent at 30 °C (see Scheme 1). To minimize the well-known problem of chain transfer to polymer during acrylic polymerization,[60] a low-temperature redox initiator based on KPS and AsAc[61−63] at pH 3 or KPS and *N*,*N*,*N*′,*N*′-tetramethylethylenediamine (TMEDA) at pH 7 was employed at a [DDMAT]/[KPS] molar ratio of 5.0. ^{1}H NMR studies confirmed good reproducibility when conducting this first step at pH 3: the PNAEP precursor had a mean DP of 85 ± 1 and 96 ± 1% NAEP conversion was achieved within just 10 min at 30 °C; these data are averaged over the 30 PNAEP precursors that were used to construct the pseudo-phase diagram (see later). Dimethyl formamide gel permeation chromatography (DMF GPC) analysis of the aliquots extracted from the reaction solution for ^{1}H NMR analysis confirmed good

https://doi.org/10.1021/acs.chemmater.1c02096
Chem. Mater. XXXX, XXX, XXX−XXX

Scheme 2. Intermolecular Crosslinking of PHBA Chains within PNAEP$_{85}$-PHBA$_x$ Diblock Copolymer Nano-Objects (In This Case, Spheres) via Acid-Catalyzed Nucleophilic Attack of Pendent Hydroxyl Groups by Glutaraldehyde (GA)[a]

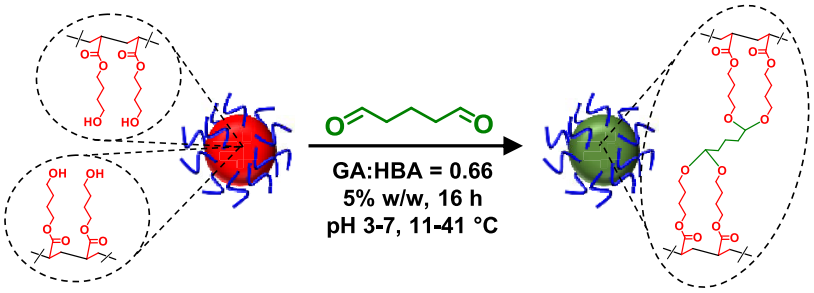

[a]This enabled a range of PNAEP$_{85}$-PHBA$_x$ nano-objects to be covalently stabilized under various conditions (e.g., pH 3−7, 11−41 °C).

reproducibility for the target M_n of the 30 PNAEP$_{85}$ precursors prepared via RAFT aqueous solution polymerization (19.1 ± 0.4 kg mol^{-1}; Figure S1). Moreover, each precursor had a relatively narrow molecular weight distribution (M_w/M_n < 1.20; Figure S1). [N.B. The KPS/TMEDA redox initiator was also employed to prepare the PNAEP$_{85}$ precursor at pH 7, with ^{1}H NMR and DMF GPC analysis (see Figure S2b), indicating that essentially the same precursor was obtained compared to that synthesized at pH 3.]

The kinetics for the subsequent RAFT aqueous dispersion polymerization of HBA at 30 °C were examined when targeting a PNAEP$_{85}$-PHBA$_{435}$ diblock copolymer at either pH 3 or pH 7 (see Figure S2). ^{1}H NMR studies were used to monitor the disappearance of vinyl signals at 5.8 and 6.4 ppm relative to the integrated two oxymethylene protons at 4.2−4.3 ppm assigned to the growing PHBA block (see Figure S3). These studies indicated that more than 95% conversion was achieved within 60 min for the synthesis at pH 3 and within 120 min at pH 7 when targeting 20% w/w solids at 30 °C. DMF GPC analysis indicated good RAFT control in both cases, with slightly lower blocking efficiencies being achieved at pH 7 (see Figure S4). GPC analysis using either a refractive index detector or a UV detector indicated the presence of a high molecular weight shoulder in each case (see Figure S5). This is consistent with chain transfer to polymer during the RAFT aqueous dispersion polymerization of HBA, even though such syntheses were conducted at 30 °C. Indeed, literature precedent suggests that this side reaction occurs even under such mild conditions.[60,64,65]

It is perhaps worth noting that the similarity between the RI and UV GPC traces indicates that essentially all of the copolymer chains retain their living character. This was expected owing to the greater hydrolytic stability afforded by trithicarbonate-based CTAs (such as the DDMAT employed in this study) compared to that of dithioesters.[66−68] Moreover, performing these syntheses under mild conditions (e.g., 30 °C, pH 3−7) should ensure minimal loss of RAFT chain ends.

Depending on the solution pH chosen for the RAFT aqueous dispersion polymerization of HBA, dynamic light scattering (DLS) analysis indicated significant differences for the evolution in particle size (Figure S6). At pH 3, four distinct morphology regions were identified that correspond to dissolved chains, spheres, worms, and vesicles (Figure S6a). This sequence of copolymer morphologies is well established for RAFT aqueous dispersion polymerization formulations reported in the literature.[69] In striking contrast, DLS analysis of a series of aliquots periodically extracted during the RAFT dispersion polymerization of HBA conducted at pH 7 suggested that this formulation produced only spheres (Figure S6b). After nucleation (which occurs at 40% HBA conversion), the z-average diameter for these spheres increased monotonically from 26 to 43 nm throughout the rest of the polymerization. ζ-Potential studies suggested that this was the result of deprotonation of the carboxylic acid end group on each PNAEP stabilizer at pH 7, which introduces significant anionic character.[70] This is sufficient to prevent one-dimensional (1D) sphere−sphere fusion and hence leads to the formation of kinetically trapped spheres (Figure S6b).

TEM characterization of such PHBA-based nano-objects is extremely challenging. This is because the PHBA block has a relatively low T_g, as indicated by its soft, gum-like appearance at ambient temperature and confirmed by DSC analysis of a PHBA$_{300}$ homopolymer (see Figure S7). Five dried linear PNAEP$_{85}$-PHBA$_x$ diblock copolymers prepared via RAFT aqueous dispersion polymerization were also analyzed by DSC. The T_g observed for the PHBA block was reduced from −14.3 to −40.5 °C on increasing its DP (x) from 125 to 525 (Figure S8), which is contrary to the trend predicted by the Fox equation.[71] However, this relationship assumes that there are no specific interactions between the comonomer repeat units, whereas strong hydrogen bonding between the pyrrolidone rings within the PNAEP block and the hydroxyl groups on the HBA repeat units almost certainly occurs in the solid state (see Figure S9 for Fourier transform infrared (FT-IR) spectra and corresponding text).[72] The low T_g values recorded for the PHBA block (Figures S7 and S8) invariably led to film formation on the TEM grid (Figure S10a), which makes the original linear copolymer morphology impossible to assess.

Glutaraldehyde (GA) is a water-soluble reagent that is widely used as a crosslinker for various biomedical applications,[73,74] including the covalent stabilization of proteins to facilitate their characterization by electron microscopy.[75−77] GA has also been used to crosslink various water-soluble polymers.[78−83] However, as far as we are aware, this reagent has not been previously used to crosslink thermoresponsive diblock copolymer nanoparticles. GA can undergo a remarkable range of reactions in aqueous solution, producing a complex mixture of monomeric GA, unsaturated polymeric GA and cyclic GA species.[73,75−77,84−88] The major species depends on both the initial GA concentration and the solution pH.[74] The crosslinking of proteins using GA is not fully understood but is believed to involve multiple mechanisms, including Schiff base chemistry to form imine bonds[84,88] and Michael addition of protein-based amine groups to α,β-unsaturated aldehydes formed by aldol condensation of GA.[85,86] Intramolecular crosslinks are favored over intermo-

https://doi.org/10.1021/acs.chemmater.1c02096
Chem. Mater. XXXX, XXX, XXX−XXX

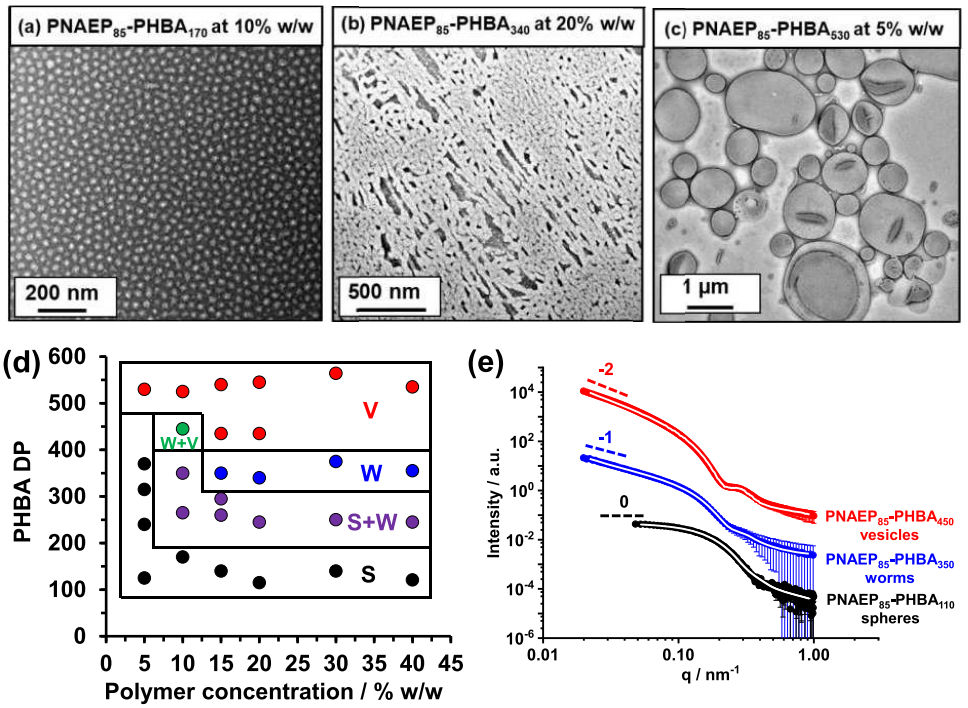

Figure 1. Representative TEM images recorded for: (a) GA-crosslinked $PNAEP_{85}$-$PHBA_{170}$ spheres prepared at 10% w/w; (b) GA-crosslinked $PNAEP_{85}$-$PHBA_{340}$ worms prepared at 20% w/w; and (c) GA-crosslinked $PNAEP_{85}$-$PHBA_{530}$ vesicles prepared at 5% w/w. (d) Pseudo-phase diagram constructed for $PNAEP_{85}$-$PHBA_x$ diblock copolymer nano-objects. S = pure spheres; S + W = a mixed phase comprising spheres and worms; W = pure worms; W + V = a mixed phase comprising worms and vesicles; and V = pure vesicles. Each copolymer morphology was assigned on the basis of TEM analysis of covalently stabilized nano-objects prepared using glutaraldehyde as a crosslinker at pH 3 and 22 °C (GA/HBA molar ratio = 0.66). (e) SAXS patterns (black, blue, and red symbols) and corresponding data fits (solid white lines) obtained for 1.0% w/w aqueous copolymer dispersions of linear $PNAEP_{85}$-$PHBA_{110}$ spheres, $PNAEP_{85}$-$PHBA_{350}$ worms, and $PNAEP_{85}$-$PHBA_{450}$ vesicles (each of these nano-objects was synthesized at 20% w/w solids).

lecular crosslinks when GA reacts with proteins.[76,87] However, the relative proportion of these two types of linkages depends on the concentration of both GA and the protein.[76,87] GA has also been widely investigated as a crosslinker for the acid-catalyzed synthesis of water-insoluble poly(vinyl alcohol) (PVA) membranes.[78−83] In this case, FT-IR spectroscopy studies indicated that the major product contained an acetal ring, which is produced when two pairs of neighboring secondary hydroxyl groups on PVA chains react with two aldehyde groups on GA (see Scheme 2).[89] However, monofunctional addition of GA has also been reported.[79,89] Given this extensive literature precedent, we postulated that GA should act as an effective crosslinker for PHBA-based nanoparticles in an aqueous solution by forming acetal linkages between the pendent hydroxyl groups on the weakly hydrophobic PHBA chains (Scheme 2).[74]

In principle, one GA molecule can react with four PHBA hydroxy groups to form two acetal linkages. This suggests that a GA/HBA molar ratio of 0.25 should be sufficient to afford covalently stabilized nanoparticles that do not undergo film formation during TEM grid preparation. However, it was found empirically that a GA/HBA molar ratio of 0.66 was required to ensure that good-quality TEM images were obtained (see Figure S10). FT-IR spectroscopy studies of freeze-dried GA-crosslinked $PNAEP_{85}$-$PHBA_{500}$ nano-objects indicated the formation of acetal linkages (see Figure S11).[73,75−77,84−88] Unfortunately, the addition of GA to 20% w/w aqueous dispersions of $PNAEP_{85}$-$PHBA_x$ spheres, worms or vesicles led to macroscopic gelation within 5 min when using a GA/HBA molar ratio of 0.66. To avoid this gelation problem, all crosslinking reactions were conducted at 5% w/w for 16 h (Scheme 2).

Accordingly, various copolymer morphologies were targeted at pH 3 by systematically varying the DP of the core-forming PHBA block between 100 and 550 while adjusting the copolymer concentration between 5% w/w and 40% w/w (see Table S1). GA crosslinking of the $PNAEP_{85}$-$PHBA_x$ nano-objects formed at 22 °C enabled conventional TEM analysis, see Figure 1a−c. Moreover, DSC analysis indicated that the T_g of the PHBA block (observed at around −14.3 to −40.5 °C for the original linear nano-objects) was no longer detected for GA-crosslinked nano-objects, while the T_g for the PNAEP block remained discernible (Figure S7). Furthermore, DLS studies confirmed that GA crosslinking eliminated the stimulus-responsive behavior exhibited by such nano-objects, hence preserving the copolymer morphology that is formed at any given temperature or pH (Figure S12). These TEM-assigned copolymer morphologies were used to construct a pseudophase diagram (Figures 1d and S13). SAXS patterns recorded for 1.0% w/w aqueous dispersions of linear $PNAEP_{85}$-$PHBA_{110}$, $PNAEP_{85}$-$PHBA_{350}$ and $PNAEP_{85}$-$PHBA_{450}$ nano-objects at pH 3 are shown in Figure 1e.

Unlike TEM, the SAXS data are averaged over many millions of nanoparticles, so the latter technique is expected to provide much more statistically robust information. Moreover, SAXS studies are conducted on aqueous dispersions, so GA crosslinking is not required to stabilize the copolymer morphology. The low q gradient in the SAXS pattern recorded for $PNAEP_{85}$-$PHBA_{110}$ nano-objects is close to zero, which indicates the presence of spheres.[90]

https://doi.org/10.1021/acs.chemmater.1c02096
Chem. Mater. XXXX, XXX, XXX−XXX

In contrast, the low q gradient in the SAXS pattern obtained for PNAEP$_{85}$-PHBA$_{350}$ nano-objects is close to −1, suggesting highly anisotropic worms.[18,48] Finally, a low q gradient of −2 was observed in the SAXS pattern for PNAEP$_{85}$-PHBA$_{350}$ nano-objects, which is characteristic of vesicles (or bilayers).[18,48] In each case, these findings are consistent with the corresponding TEM images (Figure 1a−c). Moreover, these three SAXS patterns could be satisfactorily fitted using well-known scattering models developed for spheres, worms and vesicles, respectively (see Table S2 for a summary of nano-object dimensions obtained when using such models).[91,92] Overall, these TEM and SAXS data demonstrate that GA crosslinking does not perturb the original copolymer morphology.

Lovett and co-workers reported that ionization of a single carboxylic acid end-group increased the volume fraction of the stabilizer block of PGMA$_{56}$-PHPMA$_{155}$ worms sufficiently to induce a worm-to-sphere transition.[70] This pH-induced change in the packing parameter, P, proved to be reversible and could be prevented by the addition of salt. Furthermore, the gradual addition of NaOH to PGMA$_{43}$-PHPMA$_{200}$ vesicles led to the irreversible formation of a free-standing worm gel. To examine whether ionization of carboxylic acid end-groups also induced a change in copolymer morphology for PNAEP$_{85}$-PHBA$_{545}$ nano-objects, GA crosslinking was conducted at pH 3, pH 5 and pH 7 prior to TEM analysis (Figure 2a).

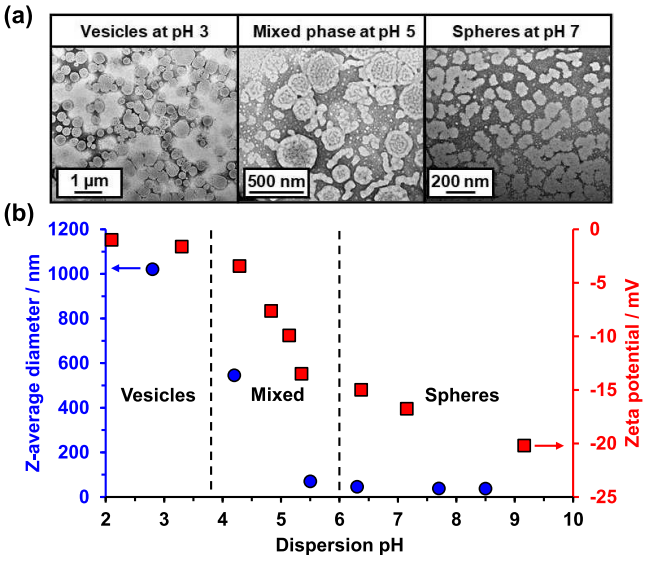

Figure 2. (a) TEM images recorded for PNAEP$_{85}$-PHBA$_{545}$ diblock copolymer nano-objects crosslinked using glutaraldehyde at 22 °C for 24 h at pH 7, pH 5 or pH 3. (b) Z-average diameter (blue squares) and ζ-potential (red squares) as a function of dispersion pH recorded for the same PNAEP$_{85}$-PHBA$_{545}$ nano-objects, where the anionic character observed above pH 4 is attributed to ionization of the carboxylic acid group located at the end of each PNAEP stabilizer chain.

The carboxylic acid end-groups are protonated at pH 3 and rather polydisperse vesicles are obtained under such conditions (z-average diameter = 1020 nm; TEM diameter = 690 ± 260 nm; see Figure 2). The dispersion pH was adjusted to pH 5 using NaOH and TEM studies indicated the formation of a mixed phase comprising vesicles and worms. According to DLS analysis, a concomitant reduction in z-average diameter occurred during this partial phase transition from vesicles to mixed vesicles/worms (Figure 2). Further addition of NaOH produced somewhat ill-defined, pseudo-spherical nano-objects at pH 7 (z-average diameter = 38 nm; TEM diameter = 87 ± 18 nm; Figure 2). The relatively large apparent number-average diameter indicated by TEM suggests that only partial GA crosslinking was achieved in this latter case, which allows some degree of nanoparticle deformation (spreading) to occur during TEM grid preparation. These observations suggest that ionization of the carboxylic acid end-group present at the end of each PNAEP stabilizer chain is sufficient to drive a vesicle-to-sphere transition. This interpretation is supported by aqueous electrophoresis data and DLS studies (see Figure 2b). Furthermore, this pH-induced transition proved to be both rapid and reversible and could not be prevented by addition of up to 1.0 M KCl (see Figure S14).

Linear PNAEP$_{85}$-PHBA$_x$ nano-objects were studied by ^{1}H NMR spectroscopy to determine the apparent degree of hydration of the structure-directing PHBA block as a function of pH (Figure 3). This involved comparing the −C$\underline{H}_2$OH

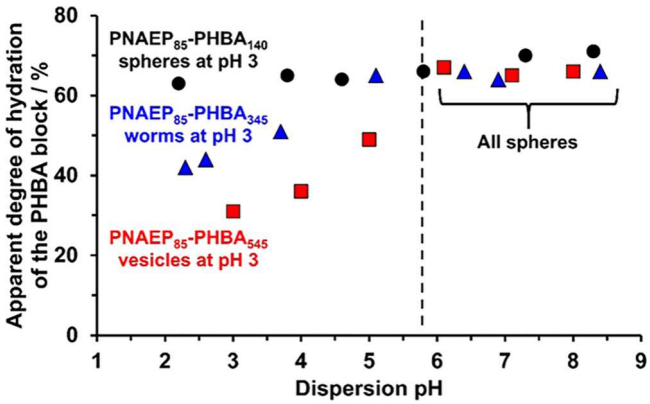

Figure 3. Apparent degree of hydration of the weakly hydrophobic PHBA block as a function of pH for linear PNAEP$_{85}$-PHBA$_x$ nano-objects at 20 °C as determined by ^{1}H NMR spectroscopy studies. [N.B. 100% hydration corresponds to the actual DP of the PHBA block, as calculated by studies of molecularly dissolved copolymer chains in CD$_3$OD (see Figure S16)].

signals assigned to the partially hydrated PHBA chains to the methylene signals assigned to pendent pyrrolidone rings on PNAEP chains. At low pH, there is a significant difference in the apparent degree of hydration of PHBA chains depending on its DP (spheres > worms > vesicles). For PNAEP$_{85}$-PHBA$_{545}$ vesicles, switching from pH 3 to pH 7 leads to a significant increase in the apparent degree of hydration of the PHBA block from 31% to 65% (Figure 3; see Figure S15 for partial ^{1}H NMR spectra), which accounts for the associated vesicle-to-sphere transition indicated by TEM studies (Figure 2a). When the PHBA block becomes more hydrated via ionization of the carboxylic acid end-group on each stabilizer chain, this induces surface plasticization of nano-objects such that HBA repeat units located near the block junction become solvated. This results in an effective increase in the volume fraction of the stabilizer block relative to that of the core block and hence a concomitant reduction in the packing parameter, which accounts for the vesicle-to-sphere transition that occurs when switching from pH 3 to pH 7. ^{1}H NMR studies of PNAEP$_{85}$-PHBA$_{340}$ worms prepared at pH 3 also indicated an increase in the apparent degree of hydration of PHBA chains on switching to pH 7, which induces a worm-to-sphere

https://doi.org/10.1021/acs.chemmater.1c02096
Chem. Mater. XXXX, XXX, XXX−XXX

transition (Figures 3 and S15). Perhaps surprisingly, ^{1}H NMR studies of PNAEP$_{85}$-PHBA$_{140}$ spheres indicated only minimal change in the degree of hydration of the PHBA block (from 65 to 70%) when switching from pH 2 to pH 8 (Figures 3 and S15). In this case, no change in copolymer morphology was observed (nor did molecular dissolution occur). This suggests that introducing a single anionic charge at the end of each PNAEP$_{85}$ stabilizer chain leads to an upper limit degree of hydration of approximately 70% for the PHBA block (see Figure 3), regardless of the PHBA DP.

Variable temperature DLS experiments were conducted on dilute aqueous dispersions of PNAEP$_{85}$-PHBA$_{295}$ nano-objects, while rheology studies were performed on 20% w/w aqueous dispersions of the same nano-objects as a function of temperature (Figure 4a). DLS studies indicated that relatively small spheres were formed between 5 and 13 °C. TEM analysis of GA-crosslinked PNAEP$_{85}$-PHBA$_{295}$ nanoparticles prepared at 11 °C (see image (i) in Figure 4b) indicates the presence of mainly spheres with a minor population of dimers and short worms. Heating from 13 to 23 °C leads to a larger z-average diameter and a higher complex viscosity ($|\eta^*|$); a maximum $|\eta^*|$ is observed at 22 °C, which corresponds to the formation of a soft, transparent free-standing gel. This is consistent with the formation of highly anisotropic worms, with a three-dimensional (3D) gel network being formed via multiple inter-worm contacts.[77] We have recently reported that the maximum $|\eta^*|$ corresponds to the presence of highly linear worms.[4] Indeed, TEM studies of GA-crosslinked nano-objects prepared at 23 °C indicate a pure worm phase with minimal branching (see image (ii) in Figure 4). Further heating led to a significant reduction in $|\eta^*|$ owing to vesicle formation (see image (iii) in Figure 4b). Heating the turbid, free-flowing vesicular dispersion above 36 °C led to another increase in $|\eta^*|$, with TEM analysis suggesting the formation of lamellae (see image (iv) in Figure 4b). The relatively soft nature of these PNAEP$_{85}$-PHBA$_x$ worm gels (G' = 24−28 Pa) is likely to be related to the highly hydrated PHBA block, which leads to flexible worm cores. Moreover, variable temperature SAXS studies conducted on a 1.0% w/w aqueous dispersion of PNAEP$_{85}$-PHBA$_{295}$ nano-objects enabled patterns to be recorded at 5, 23, 34 and 41 °C (Figure 4c). Such patterns could be satisfactorily fitted using well-known scattering models developed for spheres, worms, or vesicles, respectively.[91,92] In each case, nano-object dimensions calculated from SAXS fits were consistent with those determined by DLS and estimated by TEM (Table S3). The SAXS pattern obtained for lamellae could not be satisfactorily fitted but a mean lamellae spacing of 43 nm was calculated from the diffraction peak using $q = 2\pi/d$.

Rheological studies performed on the same 20% w/w aqueous dispersion of PNAEP$_{85}$-PHBA$_{295}$ nano-objects indicated excellent thermoreversibility for the sphere-to-worm and worm-to-vesicle transitions (see Figure S17). In contrast, significant hysteresis was observed for the lamellae-to-vesicle transition when cooling PNAEP$_{85}$-PHBA$_{295}$ lamellae from 45 °C. More specifically, vesicles were only formed at 27 °C, despite being present at up to 34 °C during the heating run (see Figure S17). Moreover, the lamellae-to-vesicle transition observed on cooling occurs at the same temperature at which the worm-to-vesicle transition is complete on heating (27 °C in Figure S17). However, further cooling indicates little or no hysteresis during the vesicle-to-worm transition, with the maximum $|\eta^*|$ being achieved at comparable temperatures (27.4 Pa·s at 22 °C on heating and 27.8 Pa·s at 21 °C on cooling). Similarly, no evidence for hysteresis was observed for the worm-to-sphere transition when cooling from 21 to 0 °C, with almost identical $|\eta^*|$ data sets being recorded for the heating and cooling cycles. This indicates that sphere-to-worm and worm-to-vesicle transitions (and also the corresponding vesicle-to-worm and worm-to-sphere transitions) both occur within the experimental timescale of 55 min allowed for the heating (and cooling) run. One might expect the associative pathway to be slower than the dissociative pathway because the former requires highly co-operative events (e.g., the stochastic 1D fusion of multiple spheres during the sphere-to-worm transition[93]). However, in both cases, the highly mobile nature

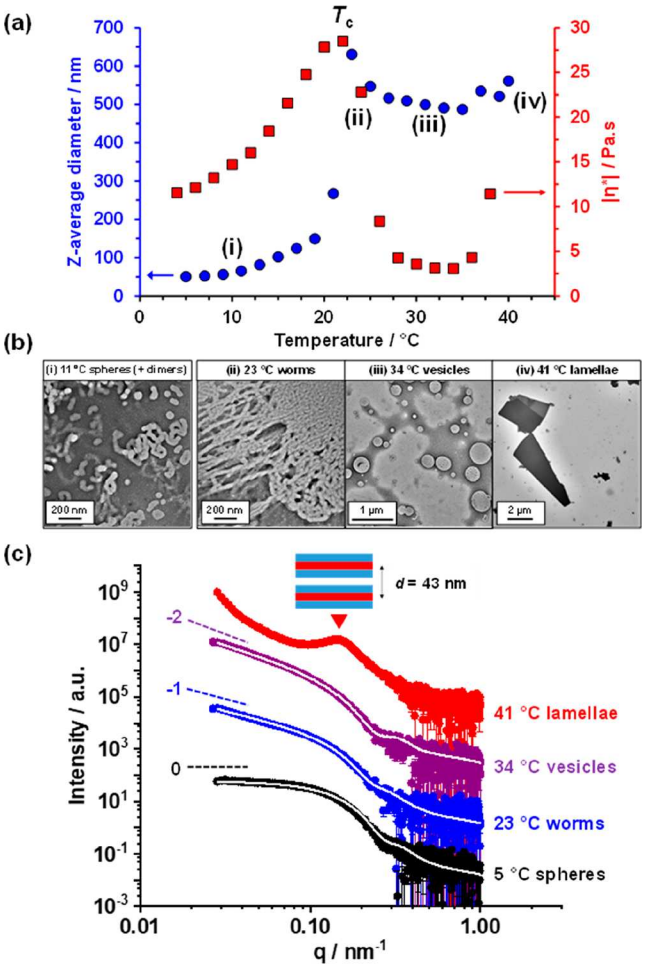

Figure 4. (a) Variation in z-average diameter (blue circles) and complex viscosity (red squares) with temperature for an aqueous dispersion of linear PNAEP$_{85}$-PHBA$_{295}$ nano-objects. DLS studies were conducted on 0.1% w/w aqueous dispersions, while rheological measurements were performed on a 10% w/w aqueous dispersion at an applied strain of 1.0% and an angular frequency of 1.0 rad s^{-1} during a run starting at 1 °C (15 min was allowed for thermal equilibration at this initial temperature prior to heating). (b) Prior to TEM analysis, 5% w/w aqueous dispersions of PNAEP$_{85}$-PHBA$_{295}$ nanoparticles were crosslinked with glutaraldehyde for 24 h at (i) 11 °C, (ii) 23 °C, (iii) 34 °C or (iv) 41 °C. (c) Small-angle X-ray scattering patterns recorded for a 1.0% w/w aqueous dispersion of linear thermoresponsive PNAEP$_{85}$-PHBA$_{295}$ nano-objects at 5 °C (black data), 23 °C (blue data), 34 °C (purple data) and 41 °C (red data; red triangle indicates the diffraction peak used to calculate D). The white lines indicate data fits obtained using appropriate scattering models (see the Supporting Information for further details).

https://doi.org/10.1021/acs.chemmater.1c02096
Chem. Mater. XXXX, XXX, XXX−XXX

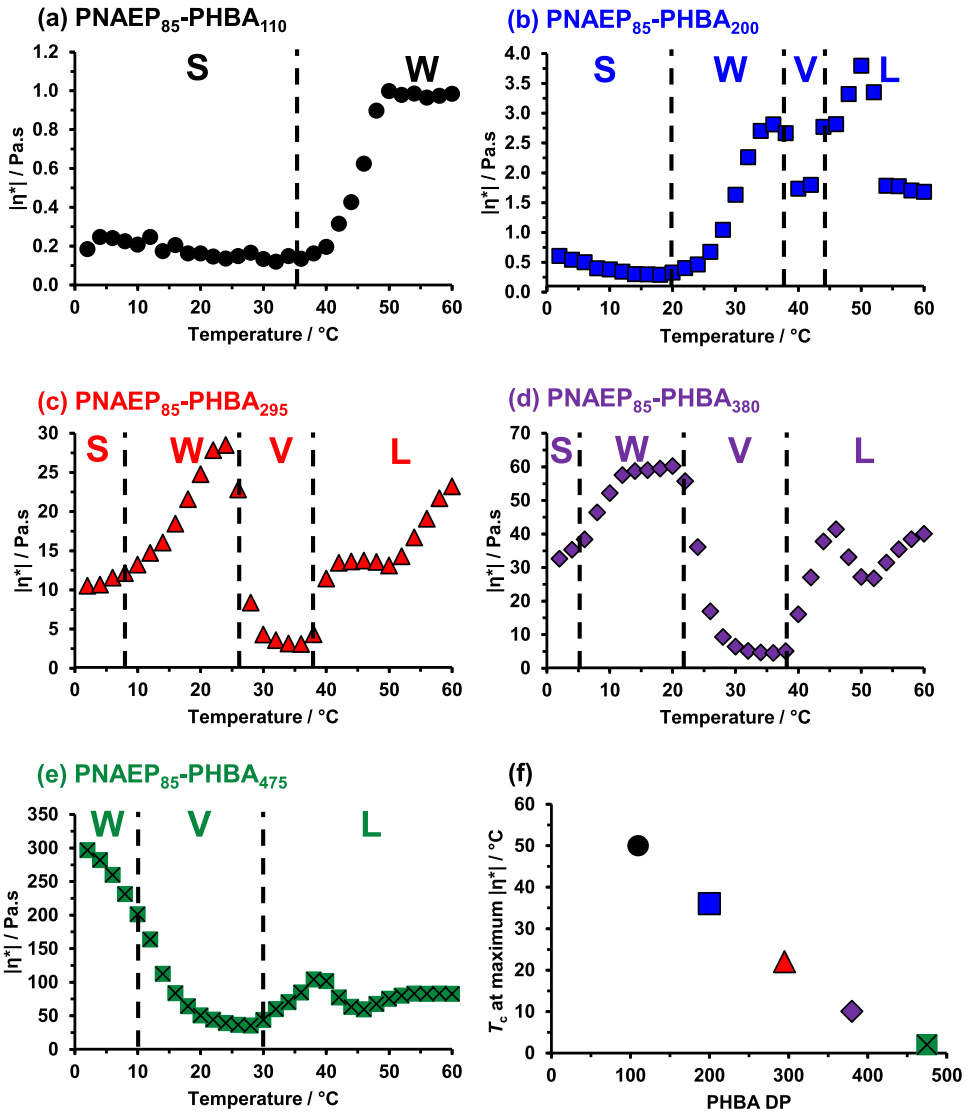

Figure 5. Variable temperature complex viscosity measurements for 20% w/w aqueous dispersions of $PNAEP_{85}$-$PHBA_x$ nano-objects at pH 3 using an applied strain of 1.0% and an angular frequency of 1.0 rad s^{-1}: (a) x = 110, (b) x = 200, (c) x = 295, (d) x = 380 and (e) x = 475. Dashed lines indicate the inferred copolymer morphology at specific temperatures (S = spheres, W = worms, V = vesicles and L = lamellae). These assignments are based on the data shown in Figure 4 and are consistent with a recent study by Byard et al.[18] (f) Relationship between the critical temperature (T_c) corresponding to the maximum $|\eta^*|$ and the PHBA DP for the same five aqueous dispersions of $PNAEP_{85}$-$PHBA_x$ nano-objects.

of the partially hydrated PHBA chains enables each of these four morphology transitions to occur within 5−10 min.

In principle, systematic variation of the PHBA DP should enable the critical temperature, T_c, for such morphology transitions to be tuned.[94] This important point is illustrated in Figure 5, which shows the rheological behavior observed for five different $PNAEP_{85}$-$PHBA_x$ nano-objects (where x = 110, 200, 295, 380 or 475). In particular, a large increase in $|\eta^*|$ occurs when these thermoresponsive nano-objects undergo a sphere-to-worm transition (see Figure 5a−d).[18,95] For a PHBA DP of 110, the T_c for this transition is around 50 °C (see Figure 5a). However, longer PHBA blocks exhibit lower T_c values (see Figure 5b−d). It is also noteworthy that heating $PNAEP_{85}$-$PHBA_{110}$ nano-objects up to 60 °C resulted in no further morphological transitions being observed. In striking contrast, the rheology data obtained for $PNAEP_{85}$-$PHBA_{200}$ suggests the formation of spheres between 10 and 20 °C, worms at around 37 °C, vesicles at approximately 40 °C and lamellae at 50 °C. Interestingly, these worms exhibit a maximum $|\eta^*|$ at around physiological temperature. In principle, this may be useful for potential biomedical applications, e.g., long-term cell culture within a wholly synthetic 3D matrix[96] or stasis induction studies.[97,98] However, these rheological experiments were conducted at pH 3. Nevertheless, it should be feasible to similarly tune the critical temperature required for maximum $|\eta^*|$ (i.e., for the formation of highly linear worms) at physiological pH in the presence of a suitable cell culture medium (e.g., PBS or Nutristem). Clearly, such optimization would require using an alternative RAFT agent that did not contain a carboxylic acid group.[99]

Returning to Figure 5, increasing the PHBA DP changes the preferred copolymer morphology at 20 °C from spheres (x = 110 or 200) to worms (x = 295 or 380) to vesicles (x = 475). In the latter case, the copolymer dispersion had to be cooled to 2 °C to partially dehydrate the PHBA block and hence induce a vesicle-to-worm transition. It is perhaps worth emphasizing here that PHPMA-based nano-objects with DPs greater than 220 exhibit no discernible thermoresponsive behavior owing to

https://doi.org/10.1021/acs.chemmater.1c02096
Chem. Mater. XXXX, XXX, XXX−XXX

the significantly greater hydrophobic character of this block.[48,94,100] Finally, an inverse linear correlation is observed between T_c and the PHBA DP over a wide temperature range (2−50 °C), see Figure 5f. In principle, this relationship can be used to predict T_c for other diblock copolymer compositions by interpolating between x values.

CONCLUSIONS

A series of PNAEP$_{85}$-PHBA$_x$ nano-objects have been prepared via redox-initiated RAFT aqueous dispersion polymerization of HBA at 30 °C using a highly efficient and reproducible one-pot protocol. High HBA conversions could be achieved within 60 min at pH 3 and within 120 min at pH 7. In both cases, DMF GPC analysis indicated a linear evolution in copolymer molecular weight with conversion, as expected for a well-controlled RAFT polymerization. However, relatively broad molecular weight distributions (M_w/M_n ∼ 1.2−2.1) are obtained, particularly when targeting higher PHBA DPs. This is attributed to chain transfer to polymer, which is well documented for acrylic monomers even at relatively low reaction temperatures.[60,64,101]

To enable assignment of copolymer morphologies, PNAEP$_{85}$-PHBA$_x$ nano-objects were crosslinked using glutaraldehyde, which forms acetal linkages between pendent hydroxyl groups on PHBA chains. Careful optimization of the copolymer concentration and glutaraldehyde/HBA molar ratio enabled such covalent stabilization to be conducted at pH 3−7 over a wide temperature range. For example, the TEM studies of the resulting crosslinked nano-objects confirmed that pure spheres, worms and vesicles could be obtained at 20 °C and pH 3 by adjusting the target diblock copolymer composition. Systematic variation of the PHBA DP between 100 and 550 while targeting copolymer concentrations of 5−40% w/w enabled the construction of a pseudo-phase diagram.

TEM studies of crosslinked PNAEP$_{85}$-PHBA$_{545}$ nano-objects prepared while varying the dispersion pH at 20 °C indicated that the copolymer morphology was pure vesicles at pH 3, a mixed phase comprising spheres, worms and vesicles at pH 5 and pure spheres at pH 7. ^{1}H NMR studies of linear PNAEP$_{85}$-PHBA$_x$ nano-objects suggest that this pH-driven shift in copolymer morphology is driven by surface plasticization of PHBA cores, which occurs on raising the dispersion pH above the pK_a of carboxylic acid end-groups located on each PNAEP$_{85}$ stabilizer chain. This introduces sufficient anionic charge to drive a vesicle-to-sphere transition via an overall reduction in the fractional packing parameter despite the higher degree of (partial) hydration of the PHBA block. On the other hand, *uniform* plasticization of PHBA chains occurs on heating at pH 3, which increases the fractional packing parameter and hence drives sphere-to-worm, worm-to-vesicle and vesicle-to-lamellae transitions. Clearly, this new PISA formulation exhibits rich self-assembly behavior despite the relatively broad molecular weight distributions obtained for diblock copolymer chains.

Rheology, DLS and TEM studies were conducted on aqueous dispersions of five examples of PNAEP$_{85}$-PHBA$_x$ nano-objects as a function of temperature. This series of experiments indicates that the critical temperature corresponding to the maximum complex viscosity ($|\eta^*|$), which indicates the formation of highly linear worms, can be tuned by systematically varying the PHBA DP. Furthermore, $|\eta^*|$ could be adjusted from 1 to 297 Pa·s and there is an inverse linear relationship between this critical temperature and the PHBA DP over a relatively wide temperature range (2−50 °C).

Given their anticipated biocompatibility, we envisage that next-generation PNAEP$_x$-PHBA$_y$ worm gels comprising neutral (e.g., ester- or amide-capped) chain ends are likely to offer new opportunities as wholly synthetic 3D matrices for long-term cell culture studies[96] or possibly for inducing stasis in embryonic human stem cells.[97,98] However, for this potential application to be realized, such PISA formulations need to be optimized to produce free-standing thermoresponsive worm gels at pH 7, rather than at pH 3.

EXPERIMENTAL SECTION

Materials. 2-(*N*-Acryloyloxy)ethyl pyrrolidone (NAEP; 95%) was provided by Ashland Specialty Ingredients (Cherry Hill, NJ) and purified by dilution with chloroform followed by sequential washes with 5% Na_2CO_3 solution, saturated NaCl solution, and finally deionized water. This aqueous solution was then dried over anhydrous $MgSO_4$ and concentrated prior to use. HBA was kindly donated by BASF (Ludwigshafen, Germany) and was purified via extraction using *n*-hexane (20 times) to remove diacrylate impurities. All chemicals used for NAEP and HBA purification were purchased from Sigma-Aldrich (Dorset, U.K.) and were used as received. *N*,*N*,*N*′,*N*′-Tetramethylethylenediamine (TMEDA), ascorbic acid (AsAc), potassium persulfate (KPS), 3-(trimethylsilyl)-1-propanesulfonic acid sodium salt (DSS), glutaraldehyde (GA; supplied as a 50% w/w aqueous solution), and 2-(dodecylthiocarbonothioylthio)-2-methylpropionic acid (DDMAT; 98%) were purchased from Sigma-Aldrich (Dorset, U.K.). CD_3OD and D_2O were purchased from Goss Scientific Instruments Ltd. (Cheshire, U.K.). All other solvents were purchased from Fisher Scientific (Loughborough, U.K.) and were used as received. Deionized water was used for all experiments.

One-Pot Synthesis of PNAEP$_{85}$-PHBA$_x$ Diblock Copolymer Nano-Objects via RAFT Aqueous Dispersion Polymerization. A typical protocol used for the one-pot synthesis of PNAEP$_{85}$-PHBA$_{435}$ diblock copolymer nano-objects at 20% w/w solids was as follows: DDMAT RAFT agent (5.30 mg, 14.6 μmol) was added to NAEP (0.200 g, 1.09 mmol; target PNAEP DP = 75) and KPS (0.80 mg, 2.9 μmol; [DDMAT]/[KPS] molar ratio = 5.0) was weighed into a 28 mL glass vial charged with a magnetic flea. This vial was then placed in an ice bath and nitrogen was passed over the top of the solution for 30 min. After 30 min, the vial was immersed in an oil bath set at 30 °C. AsAc (0.50 mg, 2.9 μmol; [DDMAT]/[AsAc] molar ratio = 5.0; [KPS]/[AsAc] molar ratio = 1.0) and acidified deionized water (57.0 mg; pH 3; final solids concentration = 78% w/w) were combined and degassed before being added via a degassed syringe/needle to the vial under a nitrogen atmosphere. The NAEP polymerization was allowed to proceed for 10 min prior to dilution of the viscous aqueous reaction solution via the addition of degassed acidified water (5.85 g; pH 3; final target solids concentration = 20% w/w). The resulting reaction solution was stirred magnetically for 2 min to ensure that the PNAEP homopolymer became fully solubilized. A degassed syringe/needle was used to extract an aliquot for ^{1}H NMR spectroscopy analysis. The disappearance of vinyl signals at 5.9 and 6.4 ppm relative to the integrated four ethyl protons at 3.4−3.8 ppm assigned to PNAEP indicated a final monomer conversion of 98%. The mean PNAEP DP was calculated to be 86 (DDMAT RAFT efficiency = 87%) as judged by ^{1}H NMR studies in CD_3OD [the integrated signal at 3.4−3.8 ppm (m, 4H) was compared with that assigned to the methyl RAFT chain-end at 0.86−0.96 ppm (t, 3H)]. DMF GPC analysis indicated an M_n of 19.2 kg mol^{-1} and an M_w/M_n of 1.16 compared to a series of 10 near-monodisperse poly(methyl methacrylate) calibration standards. To perform the second-stage polymerization, degassed HBA (1.19 g, 8.29 mmol; PHBA target DP = 435) was added to the reaction solution. KPS (1.03 mg, 3.80 μmol; [PNAEP]/[KPS] molar ratio = 5.0) and AsAc (0.67 mg, 3.80 μmol; [PNAEP]/[AsAc] molar ratio = 5.0; [KPS]/[AsAc] molar ratio = 1.0) were added to the reaction mixture

https://doi.org/10.1021/acs.chemmater.1c02096
Chem. Mater. XXXX, XXX, XXX−XXX

as dilute aqueous solutions (0.13 and 0.08 mM, respectively) using degassed syringe/needles. The HBA polymerization was allowed to proceed for 1 h at 30 °C (N.B. polymerizations targeting 5% w/w solids were allowed to run for 2 h at 30 °C) before being quenched by exposing the reaction mixture to air and immersing the glass vial into an ice bath. The extent of polymerization was determined by ^{1}H NMR spectroscopy: comparison of the integrated vinyl proton signals at 5.8 and 6.5 ppm assigned to the residual HBA monomer to the two oxymethylene protons at 4.2−4.3 ppm assigned to PHBA indicated a final HBA conversion of 98%. The mean DP of the PHBA block was calculated to be 435 as judged by ^{1}H NMR spectroscopy analysis in CD_3OD (the integrated signal at 3.6−3.8 ppm (t, 2H) was compared with that assigned to two oxymethylene protons assigned to $PNAEP_{85}$ at 2.1−2.2 ppm (m, 170H)). DMF GPC analysis indicated an M_n of 64.5 kg mol^{-1} and an M_w/M_n of 1.31. For analogous PISA syntheses, the volume of water was adjusted to afford the desired final solids concentrations. Other target diblock copolymer compositions were obtained by adjusting the [HBA]/[$PNAEP_{85}$] molar ratio.

Covalent Stabilization of the $PNAEP_{85}$-$PHBA_x$ Diblock Copolymer Nano-Objects via Crosslinking with Glutaraldehyde. A typical protocol used for crosslinking $PNAEP_{85}$-$PHBA_{255}$ spheres is as follows. A 5.0% w/w acidic aqueous dispersion of $PNAEP_{85}$-$PHBA_{255}$ spheres (0.50 g; PHBA = 121 μmol, pH 3) and glutaraldehyde (GA; 8.0 mg, 80 μmol, GA/PHBA molar ratio = 0.66) were added to a 7 mL vial. This reaction mixture was stirred at 25 °C for 16 h. Then an aliquot (10.0 mg) was extracted and diluted with water (4.99 g; final target solids' concentration = 0.05% w/w) and stirred for 24 h prior to preparation of the corresponding TEM grid (see below for further details). Crosslinking of $PNAEP_{85}$-$PHBA_{340-375}$ worms and $PNAEP_{85}$-$PHBA_{435-565}$ vesicles was also performed at 5.0% w/w; in the former case, this copolymer concentration was sufficiently low to avoid chemical gelation during crosslinking. To crosslink $PNAEP_{85}$-$PHBA_x$ diblock copolymer nano-objects at a given temperature or pH, 5.0% w/w dispersions were either equilibrated at the desired reaction temperature for 1 h or after an appropriate amount of 1 M NaOH or HCl had been added prior to GA addition. Then GA crosslinking was allowed to proceed for 16 h prior to dilution with water (final target solids concentration = 0.05% w/w) that had been pre-equilibrated at the appropriate temperature or solution pH.

COPOLYMER CHARACTERIZATION

^{1}H NMR Spectroscopy. Spectra were recorded in either CD_3OD or D_2O using a 400 MHz Bruker Avance-400 spectrometer with 64 scans being averaged per spectrum.

Gel Permeation Chromatography. Copolymer molecular weights and dispersities were determined using an Agilent 1260 Infinity GPC system equipped with both refractive index and UV−visible detectors. Two Agilent PLgel 5 μm Mixed-C columns and a guard column were connected in series and maintained at 60 °C. High-performance liquid chromatography (HPLC)-grade DMF containing 10 mM LiBr was used as the eluent and the flow rate was set at 1.0 mL min^{-1}. Refractive index detection was used for the calculation of molecular weights and dispersities by calibration against a series of 10 near-monodisperse PMMA standards (with M_n values ranging from 370 to 2 520 000 g mol^{-1}).

Transmission Electron Microscopy. Unless stated otherwise, as-prepared copolymer dispersions were diluted at 20 °C using acidified deionized water (pH 3) to generate 0.05% w/w aqueous dispersions. Copper/palladium TEM grids (Agar Scientific, U.K.) were coated in-house to produce thin films of amorphous carbon. These grids were then treated with a plasma glow discharge for 30 s to create a hydrophilic surface. One droplet of an aqueous copolymer dispersion (20 μL; 0.05% w/w) was placed on a freshly treated grid for 1 min and then blotted with a filter paper to remove excess solution. To stain deposited nanoparticles, one 10 μL droplet of a 0.75% w/w aqueous solution of uranyl formate was placed on the sample-loaded grid using a micropipet for 45 s and then carefully blotted to remove excess stain. Each grid was then dried using a vacuum hose. Imaging was performed using a Philips CM100 instrument operating at 100 kV and equipped with a Gatan 1k CCD camera.

Dynamic Light Scattering. Unless stated otherwise, measurements were conducted at 25 °C using a Malvern Instruments Zetasizer Nano ZS instrument equipped with a 4 mW He−Ne laser (λ = 633 nm) and an avalanche photodiode detector. Scattered light was detected at 173°. Copolymer dispersions were diluted to 0.10% w/w prior to analysis. Intensity-average hydrodynamic diameters were averaged over three runs and calculated using the Stokes−Einstein equation. Variable temperature studies were performed at 2 °C intervals during a 5 to 41 °C to 5 °C thermal cycle. Between each measurement, 5 min was allowed for thermal equilibration.

Aqueous Electrophoresis. ζ-Potential measurements were performed on 0.1% w/w aqueous copolymer dispersions at 20 °C in the presence of 1 mM KCl using the same Malvern Zetasizer Nano ZS instrument. The initial copolymer dispersion pH was pH 2.5 and was adjusted by the addition of small amounts of aqueous 0.1 M NaOH, with 10 min being allowed for equilibrium at each pH. ζ-Potentials were calculated from the Henry equation using the Smoluchowski approximation. Hydrodynamic DLS diameters were also recorded during these pH sweep experiments. All data were averaged over three consecutive runs.

Rheology. An AR-G2 rheometer equipped with a variable temperature Peltier plate and a 40 mL 2° aluminum cone was used for all experiments. The dispersion viscosity, loss modulus and storage modulus were measured as a function of applied strain, angular frequency and temperature to assess the gel strength, gel viscosity and critical gelation temperature. Percentage strain sweeps were conducted at 25 °C using a constant angular frequency of 1.0 rad s^{-1}. Angular frequency sweeps were conducted at the critical gelation temperature corresponding to the maximum complex viscosity using an applied strain of 1.0%. Temperature sweeps were conducted using 20% w/w copolymer dispersions at an applied strain of 1.0% and an angular frequency of 1.0 rad s^{-1}. In these latter experiments, the copolymer dispersion was subjected to a single thermal cycle (heating up to 60 °C, followed by cooling to 1 °C) and then equilibrated at 1 °C for 15 min prior to measurements. The temperature was adjusted at 2 °C intervals, allowing 60 s for thermal equilibration between each measurement.

Small-Angle X-ray Scattering Studies. SAXS patterns of 1.0% w/w aqueous diblock copolymer dispersions were recorded at a synchrotron source (Diamond Light Source, station I22, Didcot, U.K.) using monochromatic X-ray radiation (wavelength, λ = 0.124 nm, sample-to-detector distance = 9 m, such that q ranged from 0.015 to 1.3 nm^{-1}, where $q = 4\pi \sin\theta/\lambda$ is the length of the scattering vector and θ is one-half of the scattering angle) and a 2D Pilatus 2M pixel detector (Dectris, Switzerland). Alternatively, some SAXS experiments were conducted using a Xeuss 2.0 SAXS instrument (Xenocs) equipped with a FOX 3D multilayered X-ray mirror, two sets of scatterless slits for collimation, a hybrid pixel area detector (Pilatus 1M, Dectris), and a liquid gallium MetalJet X-ray source (Excillum, λ = 1.34 Å). In this case, SAXS patterns were recorded at a sample-to-detector distance of approximately 1.20 m (calibrated using a silver

https://doi.org/10.1021/acs.chemmater.1c02096
Chem. Mater. XXXX, XXX, XXX−XXX

behenate standard). Glass capillaries of 2.0 mm diameter were used as a sample holder. SAXS data were reduced (integration, normalization, and absolute intensity calibration using SAXS patterns obtained for deionized water, assuming a differential scattering cross-section for water of 0.0162 cm^{-1}) using either Dawn software supplied by Diamond Light Source or Irena SAS macros for Igor Pro.[102] The temperature was adjusted using a HFSX350-CAP temperature-controlled stage (Linkam Scientific, Tadworth, U.K.) and 10 min was allowed between each measurement to ensure thermal equilibration.

■ ASSOCIATED CONTENT

Supporting Information

The Supporting Information is available free of charge at https://pubs.acs.org/doi/10.1021/acs.chemmater.1c02096.

M_n and M_w/M_n data for $PNAEP_{85}$ precursors; kinetic data recorded during the RAFT aqueous dispersion polymerization of HBA; ^{1}H NMR spectra recorded during the RAFT aqueous dispersion polymerization of HBA; GPC traces recorded for the RAFT aqueous dispersion polymerization of HBA conducted at pH 3 and pH 7; GPC curves recorded using either a RI detector or a UV detector; *z*-average diameter vs monomer conversion; DSC curves for a $PNAEP_{85}$ homopolymer, $PHBA_{300}$ homopolymer, a GA-crosslinked $PNAEP_{85}$-$PHBA_{350}$, and a series of $PNAEP_{85}$-$PHBA_x$ diblock copolymers; FT-IR spectra recorded for freeze-dried powders of the $PHBA_{200}$ homopolymer, $PNAEP_{85}$-$PHBA_{200}$ diblock copolymer, and $PNAEP_{85}$ homopolymer; TEM images recorded for linear and GA-crosslinked $PNAEP_{85}$-$PHBA_{265}$; FT-IR spectra recorded for freeze-dried powders of the linear and crosslinked $PNAEP_{85}$-$PHBA_{265}$; summary table of diblock compositions, HBA conversions, molecular weight data, DLS particle diameters, DLS polydispersities, and TEM assignments; DLS studies of linear and crosslinked $PNAEP_{85}$-$PHBA_x$ nano-objects as a function of temperature and pH; TEM images for all GA-crosslinked $PNAEP_{85}$-$PHBA_x$ nano-objects; summary table of DLS, SAXS, and TEM data obtained for $PNAEP_{85}$-$PHBA_x$ nano-objects at pH 3 and 20 °C; digital photographs of the reversible vesicle-to-sphere transition; partially assigned ^{1}H NMR spectra recorded at various solution pH; ^{1}H NMR spectra for molecularly dissolved diblock copolymers; summary of DLS, SAXS, and TEM data obtained at 5, 23, 34, and 41 °C; and complex viscosity vs temperature measurements (PDF)

■ AUTHOR INFORMATION

Corresponding Author

Steven P. Armes − *Dainton Building, Department of Chemistry, University of Sheffield, Sheffield S3 7HF, U.K.*; orcid.org/0000-0002-8289-6351; Email: s.p.armes@sheffield.ac.uk

Authors

Oliver J. Deane − *Dainton Building, Department of Chemistry, University of Sheffield, Sheffield S3 7HF, U.K.*

James Jennings − *Dainton Building, Department of Chemistry, University of Sheffield, Sheffield S3 7HF, U.K.*

Thomas J. Neal − *Dainton Building, Department of Chemistry, University of Sheffield, Sheffield S3 7HF, U.K.*

Osama M. Musa − *Ashland Specialty Ingredients, Bridgewater, New Jersey 08807, United States*

Alan Fernyhough − *Ashland Specialty Ingredients, Bradford BD9 4SH, U.K.*

Complete contact information is available at: https://pubs.acs.org/10.1021/acs.chemmater.1c02096

Notes

The authors declare no competing financial interest.

■ ACKNOWLEDGMENTS

EPSRC is thanked for funding a CDT Ph.D. studentship for the first author (EP/L016281). Ashland Specialty Ingredients (Bridgewater, New Jersey) is thanked for financial support of this Ph.D. project, for supplying the NAEP monomer, and for permission to publish this work. S.P.A. also thanks the EPSRC for an Established Career Particle Technology Fellowship (EP/R003009).

■ REFERENCES

(1) Zhang, L.; Eisenberg, A. Multiple Morphologies of "Crew-Cut" Aggregates of Polystyrene-b-Poly(Acrylic Acid) Block Copolymers. *Science* **1995**, *268*, 1728−1731.

(2) Abbas, S.; Li, Z.; Hassan, H.; Lodge, T. P. Thermoreversible Morphology Transitions of Poly(Styrene-b-Dimethylsiloxane) Diblock Copolymer Micelles in Dilute Solution. *Macromolecules* **2007**, *40*, 4048−4052.

(3) Kim, S. Y.; Lee, K. E.; Han, S. S.; Jeong, B. Vesicle-to-Spherical Micelle-to-Tubular Nanostructure Transition of Monomethoxy-Poly(Ethylene Glycol)-Poly(Trimethylene Carbonate) Diblock Copolymer. *J. Phys. Chem. B* **2008**, *112*, 7420−7423.

(4) Verber, R.; Blanazs, A.; Armes, S. P. Rheological Studies of Thermo-Responsive Diblock Copolymer Worm Gels. *Soft Matter* **2012**, *8*, 9915−9922.

(5) Won, Y.-Y.; Davis, H. T.; Bates, F. S. Giant Wormlike Rubber Micelles. *Science* **1999**, *283*, 960−963.

(6) Discher, B. M.; Won, Y.-Y.; Ege, D. S.; Lee, J. C.-M.; Bates, F. S.; Discher, D. E.; Hammer, D. A. Polymersomes: Tough Vesicles Made from Diblock Copolymers. *Science* **1999**, *284*, 1143−1146.

(7) Wang, X.; Guerin, G.; Wang, H.; Wang, Y.; Manners, I.; Winnik, M. A. Cylindrical Block Copolymer Micelles and Co-Micelles of Controlled Length and Architecture. *Science* **2007**, *317*, 644−647.

(8) Gilroy, J. B.; Gädt, T.; Whittell, G. R.; Chabanne, L.; Mitchels, J. M.; Richardson, R. M.; Winnik, M. A.; Manners, I. Monodisperse Cylindrical Micelles by Crystallization-Driven Living Self-Assembly. *Nat. Chem.* **2010**, *2*, 566−570.

(9) Charleux, B.; Delaittre, G.; Rieger, J.; D'Agosto, F. Polymerization-Induced Self-Assembly: From Soluble Macromolecules to Block Copolymer Nano-Objects in One Step. *Macromolecules* **2012**, *45*, 6753−6765.

(10) Warren, N. J.; Armes, S. P. Polymerization-Induced Self-Assembly of Block Copolymer Nano-Objects via RAFT Aqueous Dispersion Polymerization. *J. Am. Chem. Soc.* **2014**, *136*, 10174−10185.

(11) Rieger, J. Guidelines for the Synthesis of Block Copolymer Particles of Various Morphologies by RAFT Dispersion Polymerization. *Macromol. Rapid Commun.* **2015**, *36*, 1458−1471.

(12) Derry, M. J.; Fielding, L. A.; Armes, S. P. Polymerization-Induced Self-Assembly of Block Copolymer Nanoparticles via RAFT Non-Aqueous Dispersion Polymerization. *Prog. Polym. Sci.* **2016**, *52*, 1−18.

(13) Boott, C. E.; Gwyther, J.; Harniman, R. L.; Hayward, D. W.; Manners, I. Scalable and Uniform 1D Nanoparticles by Synchronous Polymerization, Crystallization and Self-Assembly. *Nat. Chem.* **2017**, *9*, 785−792.

(14) Chaduc, I.; Zhang, W.; Rieger, J.; Lansalot, M.; D'Agosto, F.; Charleux, B. Amphiphilic Block Copolymers from a Direct and One-Pot RAFT Synthesis in Water. *Macromol. Rapid Commun.* **2011**, *32*, 1270−1276.
(15) Gody, G.; Maschmeyer, T.; Zetterlund, P. B.; Perrier, S. Pushing the Limit of the RAFT Process: Multiblock Copolymers by One-Pot Rapid Multiple Chain Extensions at Full Monomer Conversion. *Macromolecules* **2014**, *47*, 3451−3460.
(16) Lesage de la Haye, J.; Zhang, X.; Chaduc, I.; Brunel, F.; Lansalot, M.; D'Agosto, F. The Effect of Hydrophile Topology in RAFT-Mediated Polymerization-Induced Self-Assembly. *Angew. Chem., Int. Ed.* **2016**, *55*, 3739−3743.
(17) Penfold, N. J. W.; Yeow, J.; Boyer, C.; Armes, S. P. Emerging Trends in Polymerization-Induced Self-Assembly. *ACS Macro Lett.* **2019**, *8*, 1029−1054.
(18) Byard, S. J.; O'Brien, C. T.; Derry, M. J.; Williams, M.; Mykhaylyk, O. O.; Blanazs, A.; Armes, S. P. Unique Aqueous Self-Assembly Behavior of a Thermoresponsive Diblock Copolymer. *Chem. Sci.* **2020**, *11*, 396−402.
(19) D'Agosto, F.; Rieger, J.; Lansalot, M. RAFT-Mediated Polymerization-Induced Self-Assembly. *Angew. Chem., Int. Ed.* **2020**, *59*, 8368−8392.
(20) Griffith, L. G.; Swartz, M. A. Capturing Complex 3D Tissue Physiology in Vitro. *Nat. Rev. Mol. Cell Biol.* **2006**, *7*, 211−224.
(21) Blanazs, A.; Verber, R.; Mykhaylyk, O. O.; Ryan, A. J.; Heath, J. Z.; Douglas, C. W. I.; Armes, S. P. Sterilizable Gels from Thermoresponsive Block Copolymer Worms. *J. Am. Chem. Soc.* **2012**, *134*, 9741−9748.
(22) Kataoka, K.; Harada, A.; Nagasaki, Y. Block Copolymer Micelles for Drug Delivery: Design, Characterization and Biological Significance. *Adv. Drug Delivery Rev.* **2001**, *47*, 113−131.
(23) Kabanov, A. V.; Batrakova, E. V.; Alakhov, V. Y. Pluronic Block Copolymers as Novel Polymer Therapeutics for Drug and Gene Delivery. *J. Controlled Release* **2002**, *82*, 189−212.
(24) Rodriguez-Hernandez, J.; Checot, F.; Gnanou, Y.; Lecommandoux, S. Toward 'Smart' Nano-Objects by Self-Assembly of Block Copolymers in Solution. *Prog. Polym. Sci.* **2005**, *30*, 691−724.
(25) Roy, D.; Cambre, J. N.; Sumerlin, B. S. Future Perspectives and Recent Advances in Stimuli-Responsive Materials. *Prog. Polym. Sci.* **2010**, *35*, 278−301.
(26) Brinkhuis, R. P.; Rutjes, F. P. J. T.; van Hest, J. C. M. Polymeric Vesicles in Biomedical Applications. *Polym. Chem.* **2011**, *2*, 1449−1462.
(27) Blackman, L. D.; Varlas, S.; Arno, M. C.; Fayter, A.; Gibson, M. I.; O'Reilly, R. K. Permeable Protein-Loaded Polymersome Cascade Nanoreactors by Polymerization-Induced Self-Assembly. *ACS Macro Lett* **2017**, *6*, 1263−1267.
(28) Growney, D. J.; Mykhaylyk, O. O.; Armes, S. P. Micellization and Adsorption Behavior of a Near-Monodisperse Polystyrene-Based Diblock Copolymer in Nonpolar Media. *Langmuir* **2014**, *30*, 6047−6056.
(29) Penfold, N. J. W.; Ning, Y.; Verstraete, P.; Smets, J.; Armes, S. P. Cross-Linked Cationic Diblock Copolymer Worms Are Super-flocculants for Micrometer-Sized Silica Particles. *Chem. Sci.* **2016**, *7*, 6894−6904.
(30) Chan, D. H. H.; Kynaston, E. L.; Lindsay, C.; Taylor, P.; Armes, S. P. Block Copolymer Nanoparticles Are Effective Dispersant for Micrometer-Sized Organic Crystalline Particles. *ACS Appl. Mater. Interfaces* **2021**, *13*, 30235−30243.
(31) Derry, M. J.; Fielding, L. A.; Armes, S. P. Industrially-Relevant Polymerization-Induced Self-Assembly Formulations in Non-Polar Solvents: RAFT Dispersion Polymerization of Benzyl Methacrylate. *Polym. Chem.* **2015**, *6*, 3054−3062.
(32) Perrier, S.; Takolpuckdee, P. Macromolecular Design via Reversible Addition-Fragmentation Chain Transfer (RAFT)/Xanthates (MADIX) Polymerization. *J. Polym. Sci., Part A: Polym. Chem.* **2005**, *43*, 5347−5393.
(33) Sugihara, S.; Blanazs, A.; Armes, S. P.; Ryan, A. J.; Lewis, A. L. Aqueous Dispersion Polymerization: A New Paradigm for in Situ Block Copolymer Self-Assembly in Concentrated Solution. *J. Am. Chem. Soc.* **2011**, *133*, 15707−15713.
(34) Zhang, X.; Boissé, S.; Zhang, W.; Beaunier, P.; D'Agosto, F.; Rieger, J.; Charleux, B. Well-Defined Amphiphilic Block Copolymers and Nano-Objects Formed in Situ via RAFT-Mediated Aqueous Emulsion Polymerization. *Macromolecules* **2011**, *44*, 4149−415.
(35) Karagoz, B.; Esser, L.; Duong, H. T.; Basuki, J. S.; Boyer, C.; Davis, T. P. Polymerization-Induced Self-Assembly (PISA)—Control over the Morphology of Nanoparticles for Drug Delivery Applications. *Polym. Chem.* **2014**, *5*, 350−355.
(36) Tan, J.; Sun, H.; Yu, M.; Sumerlin, B. S.; Zhang, L. Photo-PISA: Shedding Light on Polymerization-Induced Self-Assembly. *ACS Macro Lett.* **2015**, *4*, 1249−1253.
(37) Jiang, Y.; Xu, N.; Han, J.; Yu, Q.; Guo, L.; Gao, P.; Lu, X.; Cai, Y. The Direct Synthesis of Interface-Decorated Reactive Block Copolymer Nanoparticles via Polymerisation-Induced Self-Assembly. *Polym. Chem.* **2015**, *6*, 4955−4965.
(38) Zhou, D.; Dong, S.; Kuchel, R. P.; Perrier, S.; Zetterlund, P. B. Polymerization Induced Self-Assembly: Tuning of Morphology Using Ionic Strength and PH. *Polym. Chem.* **2017**, *8*, 3082−3089.
(39) Perrier, S. 50th Anniversary Perspective: RAFT Polymerization—A User Guide. *Macromolecules* **2017**, *50*, 7433−7447.
(40) Khor, S. Y.; Quinn, J. F.; Whittaker, M. R.; Truong, N. P.; Davis, T. P. Controlling Nanomaterial Size and Shape for Biomedical Applications via Polymerization-Induced Self-Assembly. *Macromol. Rapid Commun.* **2019**, *40*, No. 1800438.
(41) Moad, G.; Rizzardo, E.; Thang, S. H. Living Radical Polymerization by the RAFT Process—A First Update. *Aust. J. Chem.* **2006**, *59*, 669−692.
(42) Moad, G.; Rizzardo, E.; Thang, S. H. Living Radical Polymerization by the RAFT Process A Second Update. *Aust. J. Chem.* **2009**, *62*, 1402−1472.
(43) Moad, G.; Rizzardo, E.; Thang, S. H. Living Radical Polymerization by the RAFT Process—A Third Update. *Aust. J. Chem.* **2012**, *65*, 985−1076.
(44) Deane, O. J.; Lovett, J. R.; Musa, O. M.; Fernyhough, A.; Armes, S. P. Synthesis of Well-Defined Pyrrolidone-Based Homopolymers and Stimulus-Responsive Diblock Copolymers via RAFT Aqueous Solution Polymerization of 2-(N-Acryloyloxy)-Ethylpyrrolidone. *Macromolecules* **2018**, *51*, 7756−7766.
(45) Deane, O. J.; Musa, O. M.; Fernyhough, A.; Armes, S. P. Synthesis and Characterization of Waterborne Pyrrolidone-Functional Diblock Copolymer Nanoparticles Prepared via Surfactant-Free RAFT Emulsion Polymerization. *Macromolecules* **2020**, *53*, 1422−1434.
(46) An, Z.; Shi, Q.; Tang, W.; Tsung, C.-K.; Hawker, C. J.; Stucky, G. D. Facile RAFT Precipitation Polymerization for the Microwave-Assisted Synthesis of Well-Defined, Double Hydrophilic Block Copolymers and Nanostructured Hydrogels. *J. Am. Chem. Soc.* **2007**, *129*, 14493−14499.
(47) Grazon, C.; Rieger, J.; Sanson, N.; Charleux, B. Study of Poly(N,N-Diethylacrylamide) Nanogel Formation by Aqueous Dispersion Polymerization of N,N-Diethylacrylamide in the Presence of Poly(Ethylene Oxide)-b-Poly(N,N-Dimethylacrylamide) Amphiphilic Macromolecular RAFT Agents. *Soft Matter* **2011**, *7*, 3482−3490.
(48) Warren, N. J.; Mykhaylyk, O. O.; Mahmood, D.; Ryan, A. J.; Armes, S. P. RAFT Aqueous Dispersion Polymerization Yields Poly(Ethylene Glycol)-Based Diblock Copolymer Nano-Objects with Predictable Single Phase Morphologies. *J. Am. Chem. Soc.* **2014**, *136*, 1023−1033.
(49) Xu, Y.; Li, Y.; Cao, X.; Chen, Q.; An, Z. Versatile RAFT Dispersion Polymerization in Cononsolvents for the Synthesis of Thermoresponsive Nanogels with Controlled Composition, Functionality and Architecture. *Polym. Chem.* **2014**, *5*, 6244−6255.

https://doi.org/10.1021/acs.chemmater.1c02096
Chem. Mater. XXXX, XXX, XXX−XXX

(50) Figg, C. A.; Simula, A.; Gebre, K. A.; Tucker, B. S.; Haddleton, D. M.; Sumerlin, B. S. Polymerization-Induced Thermal Self-Assembly (PITSA). *Chem. Sci.* **2015**, *6*, 1230−1236.
(51) Blackman, L. D.; Doncom, K. E. B.; Gibson, M. I.; O'Reilly, R. K. Comparison of Photo- and Thermally Initiated Polymerization-Induced Self-Assembly: A Lack of End Group Fidelity Drives the Formation of Higher Order Morphologies. *Polym. Chem.* **2017**, *8*, 2860−2871.
(52) Sun, W.; An, Z.; Wu, P. Hydrogen Bonding Reinforcement as a Strategy to Improve Upper Critical Solution Temperature of Poly(N-Acryloylglycinamide-Co-Methacrylic Acid). *Polym. Chem.* **2018**, *9*, 3667−3673.
(53) Liu, D.; Cai, W.; Zhang, L.; Boyer, C.; Tan, J. Efficient Photoinitiated Polymerization-Induced Self-Assembly with Oxygen Tolerance through Dual-Wavelength Type I Photoinitiation and Photoinduced Deoxygenation. *Macromolecules* **2020**, *53*, 1212−1223.
(54) Xu, S.; Corrigan, N.; Boyer, C. Forced Gradient Copolymerisation: A Simplified Approach for Polymerisation-Induced Self-Assembly. *Polym. Chem.* **2021**, *12*, 57−68.
(55) Liu, G.; Qiu, Q.; An, Z. Development of Thermosensitive Copolymers of Poly(2-Methoxyethyl Acrylate-Co-Poly(Ethylene Glycol) Methyl Ether Acrylate) and Their Nanogels Synthesized by RAFT Dispersion Polymerization in Water. *Polym. Chem.* **2012**, *3*, 504−513.
(56) Ratcliffe, L. P. D.; Derry, M. J.; Ianiro, A.; Tuinier, R.; Armes, S. P. A Single Thermoresponsive Diblock Copolymer Can Form Spheres, Worms or Vesicles in Aqueous Solution. *Angew. Chem., Int. Ed.* **2019**, *58*, 18964−18970.
(57) Petzetakis, N.; Dove, A. P.; O'Reilly, R. K. Cylindrical Micelles from the Living Crystallization-Driven Self-Assembly of Poly(Lactide)-Containing Block Copolymers. *Chem. Sci.* **2011**, *2*, 955−960.
(58) Zhao, W.; Gody, G.; Dong, S.; Zetterlund, P. B.; Perrier, S. Optimization of the RAFT Polymerization Conditions for the in Situ Formation of Nano-Objects via Dispersion Polymerization in Alcoholic Medium. *Polym. Chem.* **2014**, *5*, 6990−7003.
(59) Mable, C. J.; Gibson, R. R.; Prevost, S.; McKenzie, B. E.; Mykhaylyk, O. O.; Armes, S. P. Loading of Silica Nanoparticles in Block Copolymer Vesicles during Polymerization-Induced Self-Assembly: Encapsulation Efficiency and Thermally Triggered Release. *J. Am. Chem. Soc.* **2015**, *137*, 16098−16108.
(60) Ahmad, N. M.; Charleux, B.; Farcet, C.; Ferguson, C. J.; Gaynor, S. G.; Hawkett, B. S.; Heatley, F.; Klumperman, B.; Konkolewicz, D.; Lovell, P. A.; Matyjaszewski, K.; Venkatesh, R. Chain Transfer to Polymer and Branching in Controlled Radical Polymerizations of N-Butyl Acrylate. *Macromol. Rapid Commun.* **2009**, *30*, 2002−2021.
(61) Misra, G. S.; Gupta, C. V. Aqueous Polymerization of Methacrylamide Initiated by the Redox System K2S2O8/Ascorbic Acid. *Die Makromol. Chem.* **1973**, *165*, 205−216.
(62) Narain, H.; Jagadale, S. M.; Ghatge, N. D. Studies of Redox Polymerization. I. Aqueous Polymerization of Acrylamide by an Ascorbic Acid−Peroxydisulfate System. *J. Polym. Sci., Polym. Chem. Ed.* **1981**, *19*, 1225−1238.
(63) Cabelli, D. E.; Bielski, B. H. J. Kinetics and Mechanism for the Oxidation of Ascorbic Acid/Ascorbate by HO2/O2- (Hydroperoxyl/Superoxide) Radicals. A Pulse Radiolysis and Stopped-Flow Photolysis Study. *J. Phys. Chem. A* **1983**, *87*, 1809−1812.
(64) Ahmad, N. M.; Heatley, F.; Lovell, P. A. Chain Transfer to Polymer in Free-Radical Solution Polymerization of n-Butyl Acrylate Studied by NMR Spectroscopy. *Macromolecules* **1998**, *31*, 2822−2827.
(65) Agirre, A.; Santos, J. I.; Etxeberria, A.; Sauerland, V.; Leiza, J. R. Polymerization of N-Butyl Acrylate with High Concentration of a Chain Transfer Agent (CBr4): Detailed Characterization and Impact on Branching. *Polym. Chem.* **2013**, *4*, 2062−2079.
(66) Baussard, J.-F.; Habib-Jiwan, J.-L.; Laschewsky, A.; Mertoglu, M.; Storsberg, J. New Chain Transfer Agents for Reversible Addition-Fragmentation Chain Transfer (RAFT) Polymerisation in Aqueous Solution. *Polymer* **2004**, *45*, 3615−3626.
(67) Thomas, D. B.; Convertine, A. J.; Hester, R. D.; Lowe, A. B.; McCormick, C. L. Hydrolytic Susceptibility of Dithioester Chain Transfer Agents and Implications in Aqueous RAFT Polymerizations. *Macromolecules* **2004**, *37*, 1735−1741.
(68) Fuchs, A. V.; Thurecht, K. J. Stability of Trithiocarbonate RAFT Agents Containing Both a Cyano and a Carboxylic Acid Functional Group. *ACS Macro Lett* **2017**, *6*, 287−291.
(69) Blanazs, A.; Madsen, J.; Battaglia, G.; Ryan, A. J.; Armes, S. P. Mechanistic Insights for Block Copolymer Morphologies: How Do Worms Form Vesicles? *J. Am. Chem. Soc.* **2011**, *133*, 16581−16587.
(70) Lovett, J. R.; Warren, N. J.; Ratcliffe, L. P. D.; Kocik, M. K.; Armes, S. P. PH-Responsive Non-Ionic Diblock Copolymers: Ionization of Carboxylic Acid End-Groups Induces an Order-Order Morphological Transition. *Angew. Chem., Int. Ed.* **2015**, *54*, 1279−1283.
(71) Fox, T. G. Influence of Diluent and of Copolymer Composition on the Glass Temperature of a Polymer System. *Bull. Am. Phys. Soc.* **1956**, *1*, No. 123.
(72) Meng, F.; Jeon, Y.-S.; Chung, D.-J.; Kim, J.-H. Miscible Blend and Semi-IPN Gel of Poly(Hydroxyethyl Aspartamide) with Poly(N-Vinyl Pyrrolidone). *Polym. Korea* **2012**, *36*, 617−621.
(73) Sabatini, D. D.; Bensch, K.; Barrnett, R. J. Cytochemistry and Electron Microscopy. *J. Cell Biol.* **1963**, *17*, 19−58.
(74) Migneault, I.; Dartiguenave, C.; Bertrand, M. J.; Waldron, K. C. Glutaraldehyde: Behavior in Aqueous Solution, Reaction with Proteins, and Application to Enzyme Crosslinking. *Biotechniques* **2004**, *37*, 790−802.
(75) Hayat, M. A. *Fixation for Electron Microscopy*, 1st ed.; Academic Press: New York, 1981.
(76) Hayat, M. A. Glutaraldehyde: Role in Electron Microscopy. *Micron Microsc. Acta* **1986**, *17*, 115−135.
(77) Kiernan, J. A. Formaldehyde, Formalin, Paraformaldehyde And Glutaraldehyde: What They Are And What They Do. *Microsc. Today* **2000**, *8*, 8−13.
(78) Kim, K.-J.; Lee, S.-B.; Han, N. W. Effects of the Degree of Crosslinking on Properties of Poly(Vinyl Alcohol) Membranes. *Polym. J.* **1993**, *25*, 1295−1302.
(79) Yeom, C.-K.; Lee, K.-H. Pervaporation Separation of Water-Acetic Acid Mixtures through Poly(Vinyl Alcohol) Membranes Crosslinked with Glutaraldehyde. *J. Membr. Sci.* **1996**, *109*, 257−265.
(80) Kurihara, S.; Sakamaki, S.; Mogi, S.; Ogata, T.; Nonaka, T. Crosslinking of Poly(Vinyl Alcohol)-Graft-N-Isopropylacrylamide Copolymer Membranes with Glutaraldehyde and Permeation of Solutes through the Membranes. *Polymer.* **1996**, *37*, 1123−1128.
(81) Rao, P. S.; Sridhar, S.; Wey, M. Y.; Krishnaiah, A. Pervaporation Performance and Transport Phenomenon of PVA Blend Membranes for the Separation of THF/Water Azeotropic Mixtures. *Polym. Bull.* **2007**, *59*, 289−298.
(82) Bolto, B.; Tran, T.; Hoang, M.; Xie, Z. Crosslinked Poly(Vinyl Alcohol) Membranes. *Prog. Polym. Sci.* **2009**, *34*, 969−981.
(83) Fan, J.-B.; Song, Y.; Wang, S.; Meng, J.; Yang, G.; Guo, X.; Feng, L.; Jiang, L. Directly Coating Hydrogel on Filter Paper for Effective Oil-Water Separation in Highly Acidic, Alkaline, and Salty Environment. *Adv. Funct. Mater.* **2015**, *25*, 5368−5375.
(84) Habeeb, A. F. S. A.; Hiramoto, R. Reaction of Proteins with Glutaraldehyde. *Arch. Biochem. Biophys.* **1968**, *126*, 16−26.
(85) Richards, F. M.; Knowles, J. R. Glutaraldehyde as a Protein Cross-Linking Reagent. *J. Mol. Biol.* **1968**, *37*, 231−233.
(86) Peters, K.; Richards, F. M. Chemical Cross-Linking: Reagents and Problems in Studies of Membrane Structure. *Annu. Rev. Biochem.* **1977**, *46*, 523−551.
(87) Cheung, D. T.; Perelman, N.; Ko, E. C.; Nimni, M. E. Mechanism of Crosslinking of Proteins by Glutaraldehyde III. Reaction with Collagen in Tissues. *Connect. Tissue Res.* **1985**, *13*, 109−115.

https://doi.org/10.1021/acs.chemmater.1c02096
Chem. Mater. XXXX, XXX, XXX−XXX

(88) Okuda, K.; Urabe, I.; Yamada, Y.; Okada, H. Reaction of Glutaraldehyde with Amino and Thiol Compounds. *J. Ferment. Bioeng.* **1991**, *71*, 100−105.
(89) Mansur, H. S.; Sadahira, C. M.; Souza, A. N.; Mansur, A. A. P. FTIR Spectroscopy Characterization of Poly (Vinyl Alcohol) Hydrogel with Different Hydrolysis Degree and Chemically Crosslinked with Glutaraldehyde. *Mater. Sci. Eng., C* **2008**, *28*, 539−548.
(90) Glatter, O.; Kratky, O. *Small Angle X-Ray Scattering*; Acedemic Press: London, 1982.
(91) Pedersen, J. S. Form Factors of Block Copolymer Micelles with Spherical, Ellipsoidal and Cylindrical Cores. *J. Appl. Crystallogr.* **2000**, *33*, 637−640.
(92) Bang, J.; Jain, S.; Li, Z.; Lodge, T. P.; Pedersen, J. S.; Kesselman, E.; Talmon, Y. Sphere, Cylinder, and Vesicle Nanoaggregates in Poly(Styrene-b-Isoprene) Diblock Copolymer Solutions. *Macromolecules* **2006**, *39*, 1199−1208.
(93) Czajka, A.; Armes, S. P. In Situ SAXS Studies of a Prototypical RAFT Aqueous Dispersion Polymerization Formulation: Monitoring the Evolution in Copolymer Morphology during Polymerization-Induced Self-Assembly. *Chem. Sci.* **2020**, *11*, 11443−11454.
(94) Warren, N. J.; Derry, M. J.; Mykhaylyk, O. O.; Lovett, J. R.; Ratcliffe, L. P. D. D.; Ladmiral, V.; Blanazs, A.; Fielding, L. A.; Armes, S. P. Critical Dependence of Molecular Weight on Thermoresponsive Behavior of Diblock Copolymer Worm Gels in Aqueous Solution. *Macromolecules* **2018**, *51*, 8357−8371.
(95) Bannister, I.; Billingham, N. C.; Armes, S. P.; Rannard, S. P.; Findlay, P. Development of Branching in Living Radical Copolymerization of Vinyl and Divinyl Monomers. *Macromolecules* **2006**, *39*, 7483−7492.
(96) Simon, K. A.; Warren, N. J.; Mosadegh, B.; Mohammady, M. R.; Whitesides, G. M.; Armes, S. P. Disulfide-Based Diblock Copolymer Worm Gels: A Wholly-Synthetic Thermoreversible 3D Matrix for Sheet-Based Cultures. *Biomacromolecules* **2015**, *16*, 3952−3958.
(97) Canton, I.; Warren, N. J.; Chahal, A.; Amps, K.; Wood, A.; Weightman, R.; Wang, E.; Moore, H.; Armes, S. P. Mucin-Inspired Thermoresponsive Synthetic Hydrogels Induce Stasis in Human Pluripotent Stem Cells and Human Embryos. *ACS Cent. Sci.* **2016**, *2*, 65−74.
(98) Sponchioni, M.; O'Brien, C. T.; Borchers, C.; Wang, E.; Rivolta, M. N.; Penfold, N. J. W.; Canton, I.; Armes, S. P. Probing the Mechanism for Hydrogel-Based Stasis Induction in Human Pluripotent Stem Cells: Is the Chemical Functionality of the Hydrogel Important? *Chem. Sci.* **2020**, *11*, 232−240.
(99) Gibson, R. R.; Armes, S. P.; Musa, O. M.; Fernyhough, A. End-Group Ionisation Enables the Use of Poly(N -(2-Methacryloyloxy)-Ethyl Pyrrolidone) as an Electrosteric Stabiliser Block for Polymerisation-Induced Self-Assembly in Aqueous Media. *Polym. Chem.* **2019**, *10*, 1312−1323.
(100) Penfold, N. J. W.; Whatley, J. R.; Armes, S. P. Thermoreversible Block Copolymer Worm Gels Using Binary Mixtures of PEG Stabilizer Blocks. *Macromolecules* **2019**, *52*, 1653−1662.
(101) Canning, S. L.; Cunningham, V. J.; Ratcliffe, L. P. D.; Armes, S. P. Phenyl Acrylate Is a Versatile Monomer for the Synthesis of Acrylic Diblock Copolymer Nano-Objects via Polymerization-Induced Self-Assembly. *Polym. Chem.* **2017**, *8*, 4811−4821.
(102) Basham, M.; Filik, J.; Wharmby, M. T.; Chang, P. C. Y.; El Kassaby, B.; Gerring, M.; Aishima, J.; Levik, K.; Pulford, B. C. A.; Sikharulidze, I.; Sneddon, D.; Webber, M.; Dhesi, S. S.; Maccherozzi, F.; Svensson, O.; Brockhauser, S.; Náray, G.; Ashton, A. W. Data Analysis WorkbeNch (DAWN). *J. Synchrotron Radiat.* **2015**, *22*, 853−858.

https://doi.org/10.1021/acs.chemmater.1c02096
Chem. Mater. XXXX, XXX, XXX−XXX